Sustainable Engineering Materials
ISSN: 3105-1960 (Print); ISSN: 3105-1979 (Online)
http://www.sustain-dpl.com/picnews.asp?id=177
DOI: 10.54113/j.suem.2025.000010

ORIGINAL ARTICLE

Size effect on the compressive properties of wood-plastic composite

Yijia Guo [a, c], Bingyu Jian[a,b], Haitao Li[a,b*], Sarah Mohrmann[a,b], Yuanjie Li[d], Jiachen Lei[a,b], Mahmud Ashraf [b,e], Jun Zhou[d]

[a] College of Civil Engineering, Nanjing Forestry University, Nanjing 210037, China
[b] Joint International Research Laboratory for Bio-composite Building Materials and Structures, Nanjing Forestry University, Nanjing 210037, China
[c] School of International Education, Tianjin Chengjian University, Tianjin 300384, China
[d] Jiangsu Qianyu WPC Technology Co., Ltd.,Yixing, 214200, China
[e] Deakin University, Geelong Waurn Ponds, VIC 3216, Australia
*Corresponding author: Haitao Li, Professor, E-mail: lhaitao1982@126.com

Abstract: Wood-plastic composite (WPC) is a kind of composite material made from a mixture of natural plant materials such as wood fibers or wood powder and special additives. The compressive strength is one of the main mechanical properties of WPC, which can be influenced by many factors. In this paper, the size effect is investigated by testing WPC specimens with proportional size and the same cross-section and different heights. The effect of specimen size on load bearing capacity, deformation capacity and strain distribution was analyzed. Based on the test data, three groups of stress-strain models for WPC were proposed. Based on Weibull brittle fracture theory, the relationship between the volume (height) parameter and compressive strength is calculated and analyzed by the parameter method, which can serve as a reference for research in related fields.

Keywords: wood-plastic composite, compressive strength, size effect, axial compression

1 Introduction

With the development of modern society and the appearance of environmental problems, the concept of green building emerged. Bamboo and wood have been increasingly studied and applied [1]. However, bamboo and wood are limited in toughness and workability due to their properties. Wood - plastic composite (WPC) combine the environmental sustainability, appearance and hardness of wood with the toughness and workability of plastic. Its main advantages include low water absorption, easy cleaning, formaldehyde-free and non-deformable cracking. As building materials, WPC can be used as outdoor paving, wall panels and formwork, as well as packaging and 3D printing materials. The raw materials for WPC are mainly thermoplastic polymers, wood fibers, wood powder, and the plastic matrix is mainly composed of polyethylene (PE), polyvinyl chloride (PVC), polypropylene (PP), polystyrene (PS), acrylonitrile - butadiene - styrene terpolymer (ABS). The raw material and matrix are processed by extrusion or remodeling. In addition, the processing of WPC also needs flame retardants, compatibilizers and coupling agents to improve its properties. **Fig. 1** shows that wood powder and wood - plastic composite products.

The WPC made of different materials has different mechanical properties. Jian et al. [2] tested the compressive strength of WPC with four formulations and found that the compression performance of the specimen with PVC plastic matrix was better than that of PE. Seyyed et al. [3] studied the effects of

Received: 4 May 2025; Received in revised form: 4 November 2025; Accepted: 30 November 2025

poplar endothelial powder (IBF), skin powder (OBF) and wood powder (WF) content on the mechanical properties of WPCs, and the results showed that the addition of WF alone resulted in higher bending strength, bending modulus and tensile strength. IBF/WF composites have higher tensile modulus, and IBF/OBF alone can improve the notch impact strength. Thanate et al. [4] studied the influence of plastic matrix on the bending properties of WPC. WPCs were made of high-density polyethylene (HDPE), low density polyethylene (LDPE), polypropylene (PP), polyvinyl chloride (PVC) and polystyrene (PS). WPCs made of PS and PP were found to have stronger bending properties than LDPE, HDPE and PVC. WPCs made of LDPE always had the weakest mechanical properties.

(a) Wood powder (b) Wood - plastic composite products

Fig. 1 Wood powder and wood - plastic composite products

WPCs made of different proportions of raw materials, particle size and fiber length have different mechanical properties. The pretreatment of raw materials and the environmental conditions also affect the mechanical properties of the composites [5-7]. Oksman et al. [8] studied the influence of humidity on the degree of crosslinking by placing the composite materials in sauna and room temperature. The results showed that the crosslinking degree of the composite was the highest in the sauna. The toughness, impact strength and creep properties of the crosslinked composites with silane were better than those of the composites without. Koay et al. [9] used recycled polystyrene (rPS) and durian shell fiber (DHF) as raw materials to study the influence of fiber content on tensile and thermal properties of rPS/DHF composites. The results showed that the higher the fiber content, the higher the tensile strength modulus and the lower the elongation at break of the composite. Irina et al. [10] compared the mechanical properties of three kinds of spruce wood powder composites. The results showed that 20 mesh wood powder composites have good bending properties.

Wang et al. [11] studied the mechanical properties of specimens processed with needle, sheet, strip and powdery fibers and found that wood needles had 4.24% higher bending strength and 7.34% lower density than sheet, strip and powdery sawdust, and that wood needles with a large aspect ratio were most suitable for producing high-performance wood-plastic materials. The mechanical properties of WPC can also be improved by pretreatment and surface modification. Zhang et al. [12] carried out hydrophobic modification of wood flour and found that the bending strength of WPC after hydrophobic modification increased by 17.3%, 26.3% and 27.5%, and the bending modulus increased by 24.4%, 24.4% and 26.0%, respectively. Zhang et al. [13] prepared PLA-based WPCs by melt blending extrusion process using polylactic acid (PLA) and wood powder as raw materials and polyethylene glycol (PEG) as compatibilizer. The results showed that with increasing PEG molecular weight, the mechanical properties of the composites first increased and then decreased.

The discovery of the size effect dates back to the renaissance in the 15th century, when Leonardo da Vinci argued that "the longest rope of the same thickness is the least strong". The size effect negates the invariable mechanical properties of materials. After continuous research, three representative size effect theories have been formed in solid mechanics: the statistical size effect theory represented by Weibull, the theory of the size effect in fracture mechanics represented by Bazant, and the multifractal size effect theory represented by Carpinteri. In 1939, Weibull [14] integrated previous research results and proposed the classical Weibull distribution. Freudenthal [15] proved the correctness of Weibull distribution by using the distribution probability model of microcracks. Bazant [16-18] believed that the size effect was mainly caused by the redistribution of stresses and the localized crack failure caused by the release of energy stored in the structure. Based on a large number of experiments, a unified

expression was proposed which was to some extent consistent with the plasticity theory or the elasticity theory. Carpinteri [19, 20] considered that the macroscopic fracture mechanics theory was no longer suitable for describing the fracture behavior due to the disordered microstructure of concrete and the interaction of various microdefects, they proposed the multifractal size effect theory.

At present, the researches on WPC mainly focus on processing methods and modification, including improving processing methods, adding modifiers to raw materials or physical and chemical methods to improve their mechanical properties and durability, but there are few researches on the application in the field of construction and size effect of WPC. In this paper, the WPCs are processed into compression components with volume of equal proportions, different height and congruent cross-section. The size effect on its mechanical properties is analyzed. The stress-strain model of WPC was proposed, and the mechanical properties of WPC were compared with those of other building materials to provide a reference for research in related fields.

2 Materials and methods

The WPCs used in this paper are from Jiangsu Qianyu WPC Technology Co., LTD. They are made of 60 mesh poplar powder and high-density polyethylene with a wood plastic ratio of 6:4, and the compatibilizer is HDPE-G-MAH. The processing method is mixing granulation and extrusion molding. The specimens in this paper are divided into five groups. The first two groups are numbered as C+W+ width + serial number, and the last three groups have cross-sections of 50 mm×50 mm, with 15 identical specimens in each group. The heights of the three groups are 50 mm, 100 mm and 150 mm, respectively. The specimen number is C+ height + serial number. For example, CW25-1 represents the first specimen with a size of 25 mm×25 mm×50 mm, and C100-1 represents the first specimen with a cross-section of 50 mm×50 mm and a height of 100 mm. The sides of the specimen are marked as A, B, C and D in a counterclockwise direction. Vertical and transverse strain gauges are pasted along the center lines of the four planes, and the symbol "×" is marked on the top surface. Two displacement gauges with a range of 50 mm were used to observe the longitudinal compression deformation of the specimens. The temperature was between 19ºC and 26ºC, and the humidity was kept basically between 44% and 74%.

Table 1 Specimens

Specimen set	Width (mm)	Thickness (mm)	Height (mm)	Number
CW25	25	25	50	15
CW30	30	30	60	15
C50	50	50	50	15
C100	50	50	100	15
C150	50	50	150	15

A universal testing machine was used and data was collected by a TDS530 static data acquisition instrument. The axial displacement was measured by two displacement meters. The loading device for the test is shown in the **Fig. 2**. First, the force control was applied and then displacement control was adopted. When the load reached about 80% of the ultimate load, it was changed to displacement control and driven at a speed of 1.2 mm/s until failure.

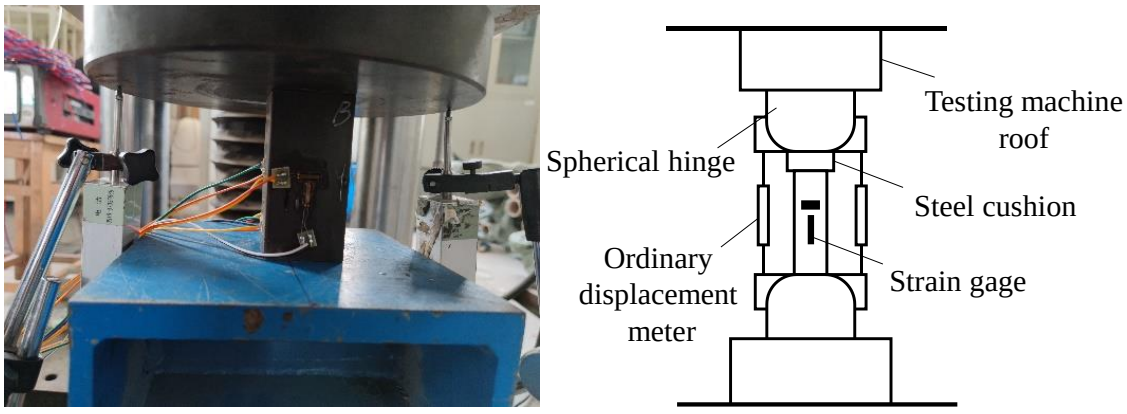

Fig. 2 Test equipment

3 Analysis of Failure Modes

There are two typical failure modes of specimens. The number of each failure mode is shown in **Table 2**.

Table 2 Number of each failure mode of the specimen

Specimen set	Model 1	Model 2	Total
CW25	12	3	15
CW30	15	0	15
C50	11	4	15
C100	12	3	15
C150	11	4	15
Total	61	14	75

3.1 Failure Mode 1

(a) Face A (b) Face B (c) Face C (d) Face D (e) Top (f) Bottom

Fig. 3 State of failure mode 1(C50-1)

Fig. 3 shows the state of the first failure mode (C50-1). At the beginning of the test there is a positive linear relationship between the displacement of the specimens and the load. There is no particular phenomenon in the elastic phase. With the increase of the axial compression load, the specimen enters the elastic-plastic phase, the axial displacement increases and the height decreases. When the load reaches about 80% of the ultimate load, the specimen starts to crack on the chamfered edge position and extends in the direction of the two sides adjacent to the centroid. After the two cracks intersect, they continue to extend axially from the intersection point to the edge line, and the specimen reaches the limit state. The cracks in the vertical plane are Y-shaped or inverted Y-shaped. Some inclined cracks of the 50-mm specimen have no intersection point or only cross and extend to the lateral line. The cracks are V-shaped or inverted V-shaped at the test duration of 10 minutes.

3.2 Failure Mode 2

(a) Face A (b) Face B (c) Face C (d) Face D (e) Top (f) Bottom

Fig. 4 State of failure mode 2(C150-3)

Fig. 4 shows the state of the second failure mode (C150-1). At the beginning of the test there is a

positive linear relationship between the displacement of the specimens and the load. There is no particular phenomenon in the elastic phase. With the increase of the axial compression load, the specimen enters the elastic-plastic phase, the axial displacement increases and the height decreases. When the load reaches about 80% of the ultimate load, the specimen starts to crack on the chamfered edge position and extends in the direction of the two sides adjacent to the centroid along the axial extension to the edge line. Then the specimen splits, the two angles split along the oblique crack, or the specimen splits along the intermediate crack. The test duration is about 10 minutes.

4 Results and Discussion

4.1 Analysis of volume and height size effect

4.1.1 Analysis of load displacement

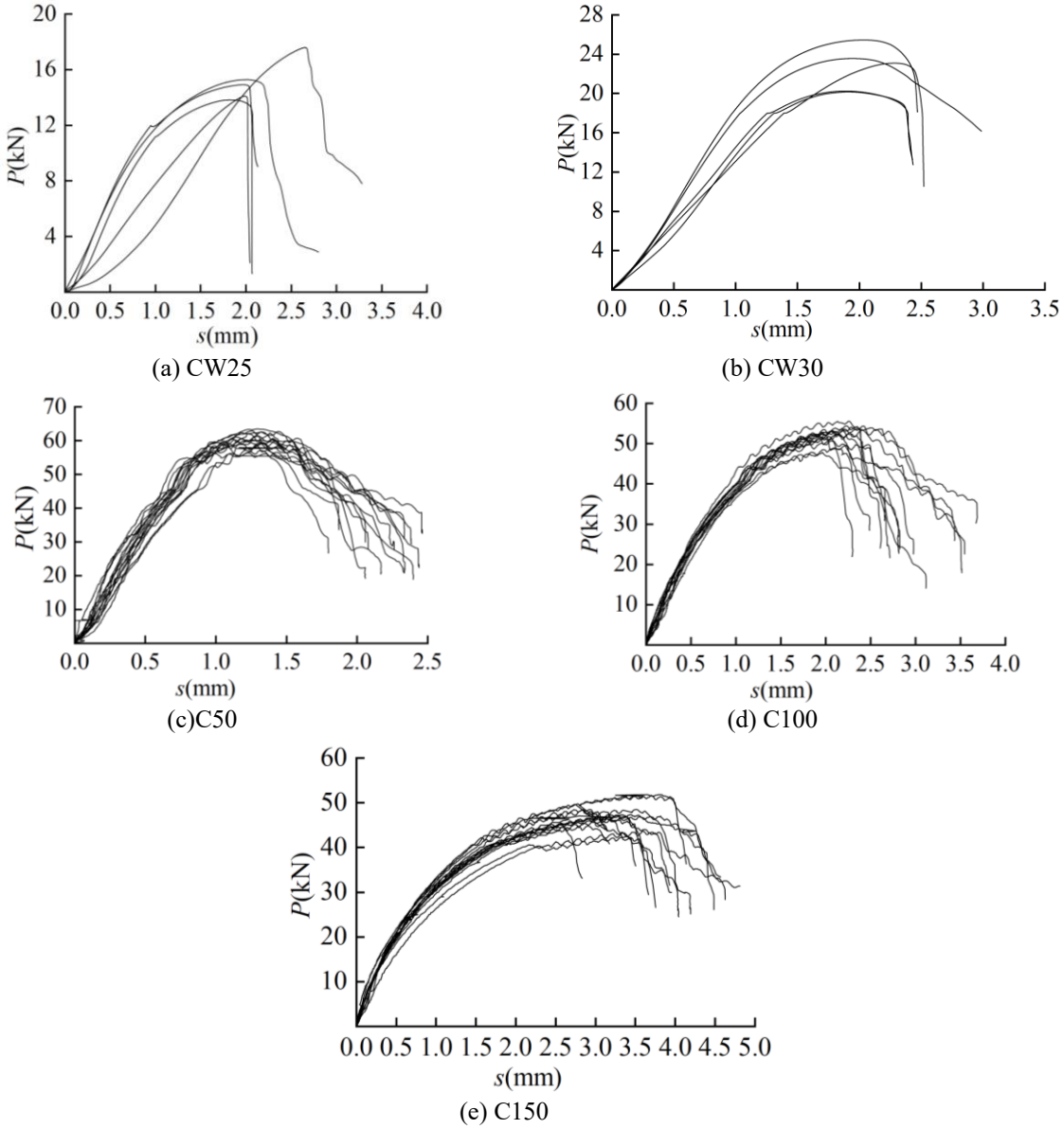

Fig. 5 Load-displacement diagrams for the specimens CW25, CW30, C50, C100 and C150

Load-displacement curves of the three groups of specimens are shown in **Fig. 5**. For CW25 and CW30, only 5 specimens in each group were obtained due to test failure.

From **Fig. 5**, it can be seen that in the initial loading stage of the specimen, most of the load-displacement changes in a linear relationship, with load and displacement showing a positive linear

correlation. When the load increases to about 80% of the ultimate load, the slope of the load-displacement curve begins to decrease, and the specimen fails when the slope of the curve decreases rapidly up to the ultimate load. From **Fig. 5**, it can be seen that the ultimate load of the CW25 specimen is between 14 kN and 18 kN, and the ultimate displacement is about 2 mm. The ultimate load of CW30 specimens is between 18 kN and 25 kN and the ultimate displacement is between 2.4 mm and 2.5 mm, the ultimate load of C50 specimens is between 52 kN and 62 kN and the ultimate displacement is between 1.2 mm and 1.4 mm, the ultimate load of C100 is between 48 kN and 55 kN and the ultimate displacement is between 2.2 mm and 2.5 mm, the ultimate load of C150 is between 42 kN and 52kN and ultimate displacement is between 3.5 mm and 4.0 mm. Therefore, the ultimate load shows a positive correlation with the volume and the ultimate displacement does not change significantly. It can also be found that there is a negative correlation between the ultimate load and specimen height and a positive correlation between the ultimate displacement and specimen height.

4.1.2 Analysis of stress and strain

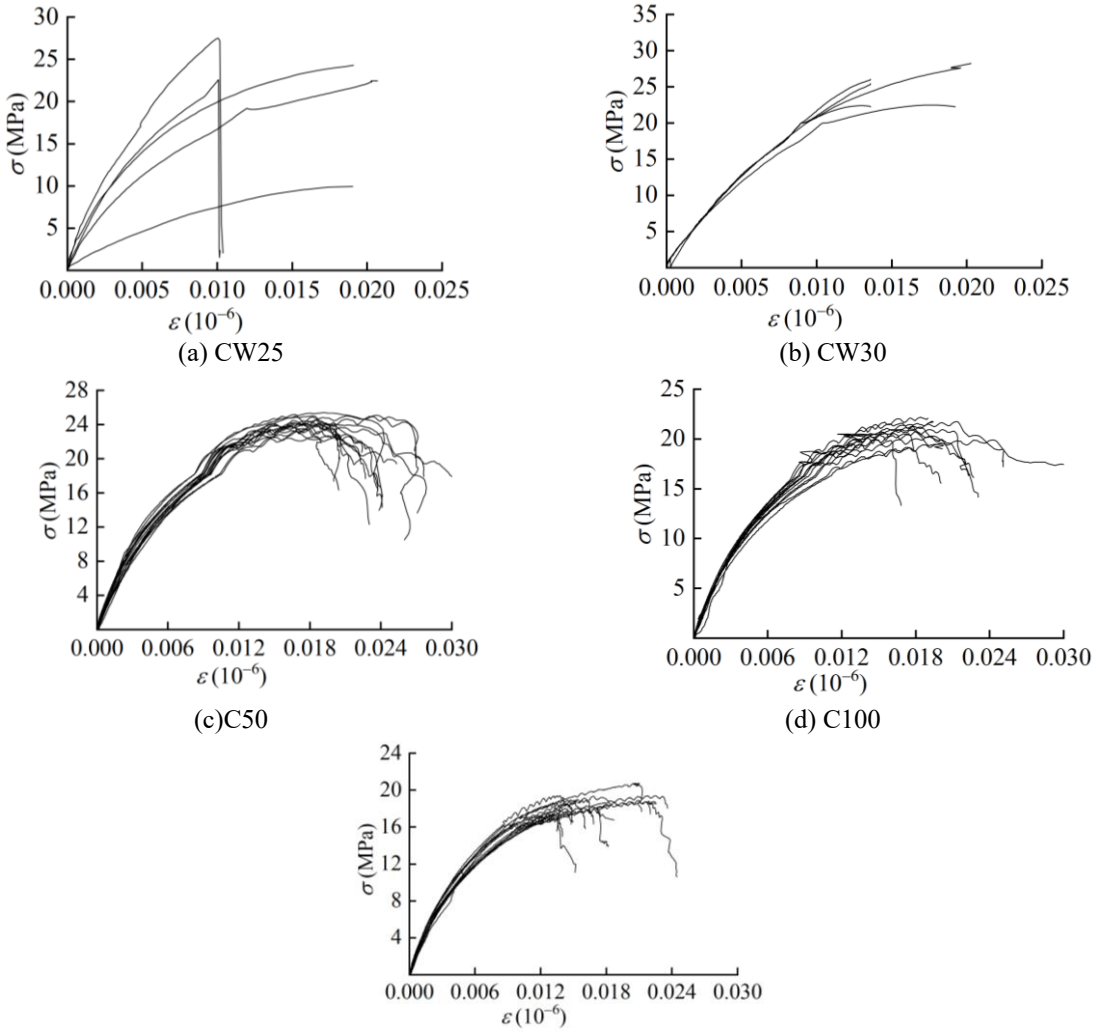

Fig. 6 Stress-strain diagrams for the specimens CW25, CW30, C50, C100 and C150

Fig. 6 shows the relationship between stress and axial strain of three groups of WPC specimens under axial load. For CW25 and CW30, only 5 specimens in each group were obtained due to test failure. From **Fig. 6**, it can be seen that as the load increases, the stress of the specimen and the axial strain increase accordingly. The trend of change can be divided into three parts. In the linear growth stage, stress and strain increase in the same ratio. In the slope reduction stage, that is, when the stress reaches about 80% of the limit stress, the speed of strain change decreases and the slope of the stress-strain curve decreases. The specimen enters the failure stage when the ultimate stress of the specimen is

reached. The bearing capacity of the specimen decreases rapidly until failure. For machine reasons, the testing of the first two groups of specimens was completed before the ultimate stress was measured, so **Fig. 6** only shows the approximate stress-strain trend and elastic modulus. It was found that the ultimate stress of C50 is 22-24MPa, that of C100 is 18-21 MPa and that of C150 is 17-19 MPa, so the ultimate stress is negatively correlated with height. CW25 has a large dispersion due to the nature of the specimen itself.

4.1.3 Analysis of the relationship between mechanical properties and volume

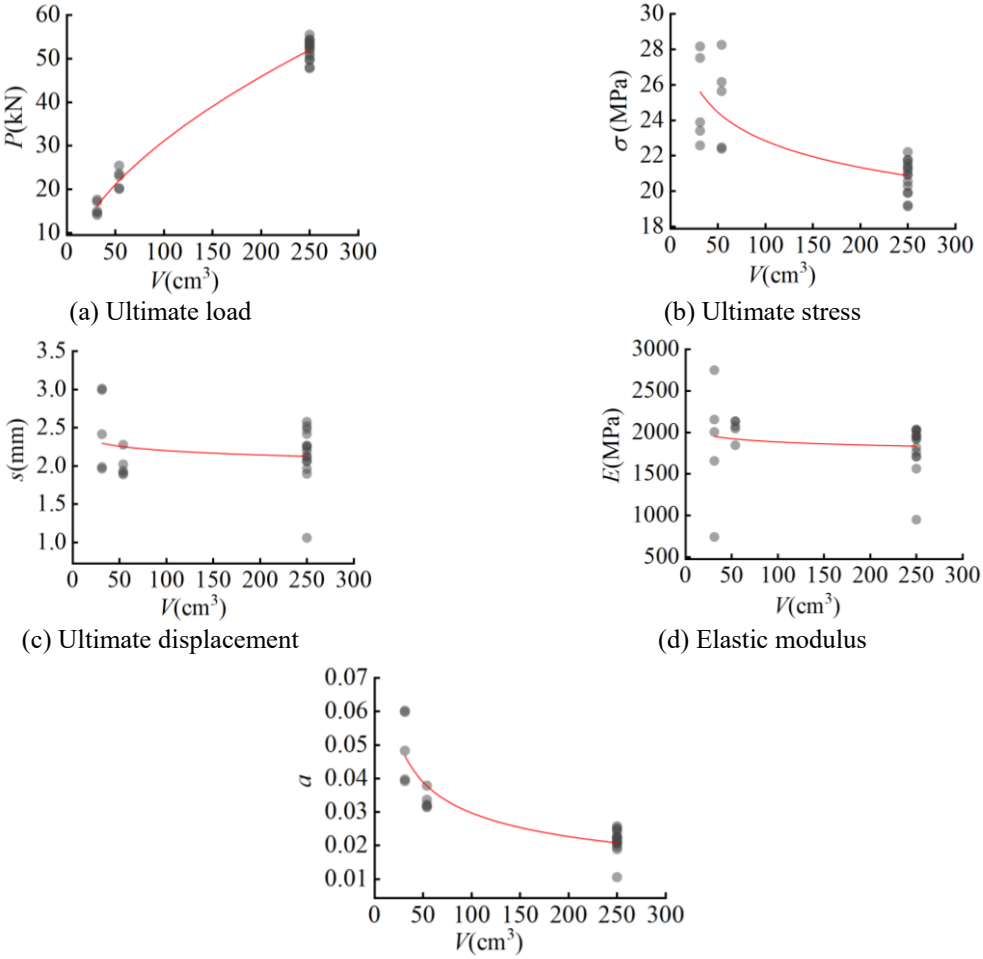

(a) Ultimate load (b) Ultimate stress

(c) Ultimate displacement (d) Elastic modulus

(e) Coefficient of compressibility

Fig. 7 Relationship between mechanical properties of specimens and volume

Fig. 7 shows the relationship between the ultimate load, ultimate displacement, ultimate stress and the elastic modulus of three groups of specimens and their volumes.

As can be seen from the **Fig. 7**, except the ultimate load increases with the increase of specimen volume, while the other three properties decrease with the increase of specimen height. In **Fig. 7(a)**, after regression analysis and calculation, the relationship between ultimate load and specimen volume can be expressed in Equation (1):

$$P = 0.049V^{0.56} \tag{1}$$

The determining coefficient: $R^2 = 0.983$.

As shown in **Fig. 7(b)**, the ultimate stress decreases with the increase of specimen height. After regression analysis and calculation, the relationship between the two can be expressed in Equation (2):

$$\sigma = 70.94V^{-0.098} \tag{2}$$

The determining coefficient: $R^2 = 0.589$.

According to the above analysis and figure, there is no obvious functional relationship between the elastic modulus, the compression coefficient and the ultimate strain and volume.

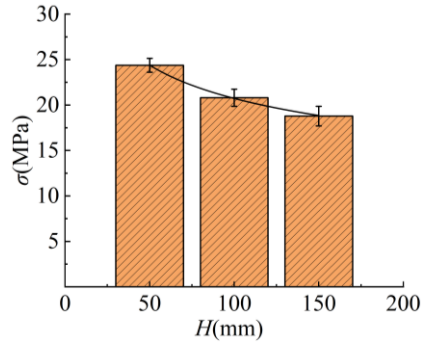

(a) Ultimate compressive strength

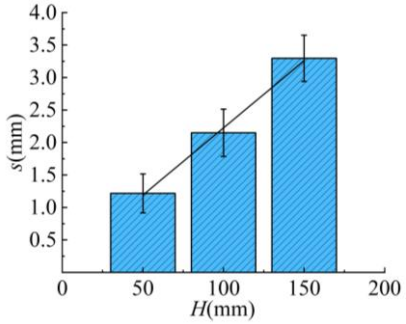

(b) Ultimate displacement

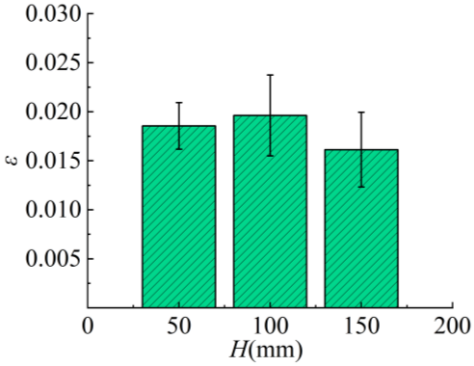

(c) Ultimate axial strain

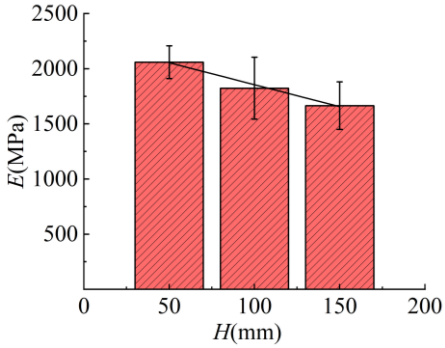

(d) Elastic modulus

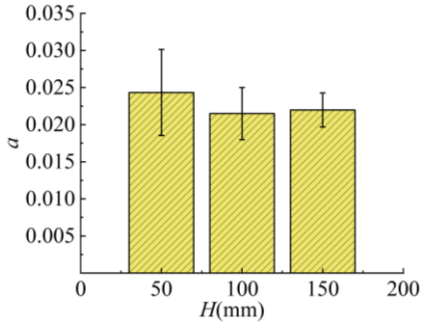

(e) Coefficient of compressibility

Fig. 8 Relationship between mechanical properties of specimens and height

4.1.4 Analysis of relationship between mechanical properties and height

Fig. 8 shows the relationship between ultimate load, ultimate displacement, ultimate stress, ultimate strain and elastic modulus of three groups of specimens and their height.

As can be seen from the **Fig. 8**, except the ultimate displacement increases with the specimen height, the other three properties all decrease with the increase of specimen height. In **Fig. 8(a)**, after regression analysis and calculation, the relationship between ultimate compressive strength and specimen height can be expressed in Equation (6):

$$\sigma = 61.09H^{-0.23} \tag{6}$$

The determining coefficient: $R^2 = 0.999$.

As shown in the **Fig. 8(b)**, the ultimate displacement increases with the increase of specimen height. After regression analysis and calculation, the relationship between the two can be expressed in Equation (7):

$$s = 0.021H + 0.16 \tag{7}$$

The determining coefficient: $R^2 = 0.993$.

As shown in the **Fig. 8(d)**, the elastic modulus decreases with the increase of specimen height. After regression analysis and calculation, the relationship between the two can be expressed in Equation (9):

$$E = -4.00H + 2254.09 \tag{9}$$

The determining coefficient: $R^2 = 0.987$.

It can be seen from the figure that the ultimate strain and compression coefficient of WPC with different heights are similar, and no obvious relationship with height is found.

The test data analysis is shown in **Table 3**.

Table 3 Statistics of test results

Group	Property index	P_{max} (kN)	s (mm)	σ_0 (MPa)	ε_{y0} (10^{-6})	ε_{x0} (10^{-6})	$\nu_{A:C}$	$\nu_{B:D}$	E (MPa)	a	ρ g/cm^3
CW25	AVG	15.70	2.48	25.11	0.010	0.0074	0.43	0.40	1863	0.0495	1.443
	SDV	1.43	2.28	2.28	0.0034	0.0012	0.097	0.072	662.694	0.00922	0.0659
	COV	0.091	0.92	0.091	0.33	0.16	0.23	0.18	0.356	0.186	0.0457
CW30	AVG	22.49	2.01	25.00	0.013	0.0088	0.46	0.48	2047	0.0334	1.441
	SDV	2.038	0.14	2.26	0.0056	0.0025	0.098	0.089	106.548	0.00238	0.0231
	COV	0.091	0.071	0.091	0.44	0.28	0.21	0.19	0.0521	0.0713	0.0161
C50	AVG	60.94	1.22	24.38	0.019	0.011	0.44	0.46	2059	0.024	1.375
	SDV	1.85	0.29	0.74	0.0023	0.0024	0.098	0.084	143.01	0.0058	0.01
	COV	0.030	0.24	0.030	0.12	0.22	0.22	0.18	0.069	0.24	0.0059
C100	AVG	52	2.15	20.80	0.020	0.0097	0.37	0.38	1823	0.022	1.35
	SDV	2.28	0.35	0.91	0.0040	0.0030	0.12	0.092	271.17	0.0035	0.0084
	COV	0.044	0.16	0.044	0.20	0.31	0.34	0.24	0.15	0.16	0.0062
C150	AVG	47.25	3.30	18.78	0.016	0.0074	0.43	0.41	1665	0.022	1.37
	SDV	2.63	0.34	1.04	0.0037	0.0020	0.36	0.080	208.26	0.0023	0.0049
	COV	0.056	0.10	0.056	0.23	0.27	0.83	0.195	0.13	0.10	0.0036

Note: P_{max} is the ultimate load, s is the ultimate displacement, σ_0 is the ultimate stress, ε_{y0} is the longitudinal ultimate strain, ε_{x0} is the transverse ultimate strain, $\nu_{A:C}$ is the average poisson's ratio of surface A and surface C, $\nu_{B:D}$ is the average poisson's ratio of surface B and surface D, E is the elasticity modulus, a is the compression coefficient, which is the ratio of ultimate displacement to original height, ρ is the density. AVG is the average, SDV is the standard deviation, COV is the coefficient of variation.

5 Theoretical Analysis

5.1 Stress-strain model

Fig. 9 shows the nonlinear relationship between stress and strain, which can be approximated by the red curves.

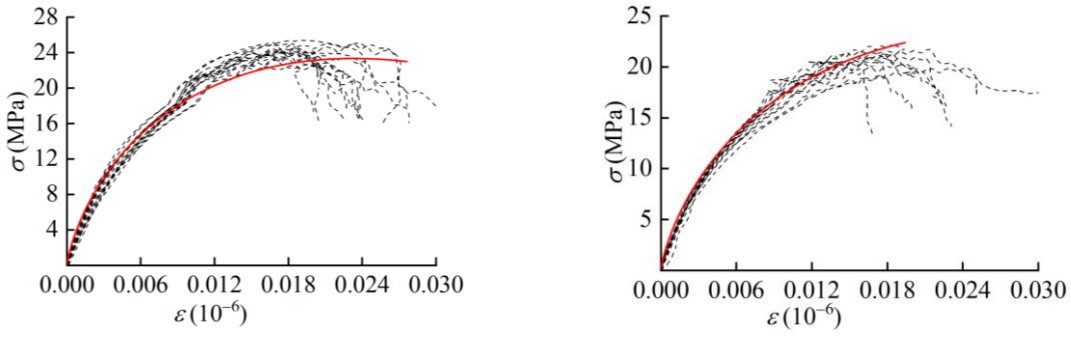

(a) C50 (b) C100

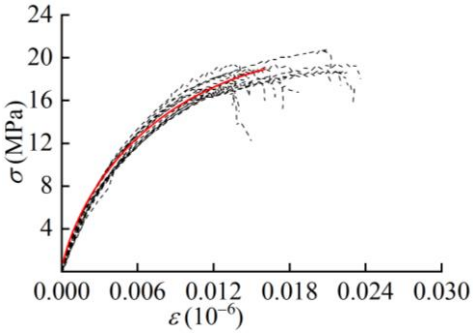

(c) C150

Fig. 9 Fitting of the stress-strain model

The stress-strain model of WPC in this paper refers to the model in [25], which can be expressed in its original form in Equation (11):

$$\varepsilon = \frac{\sigma}{E} + k\left(\frac{\sigma}{E}\right)^n \tag{11}$$

In order to make the model more consistent with the stress-strain relationship of WPC, a coefficient a is added in front of the $\frac{\sigma}{E}$ term, then the new model can be expressed as (12):

$$\varepsilon = a\frac{\sigma}{E} + k\left(\frac{\sigma}{E}\right)^n \tag{12}$$

According to Equation (12), the stress-strain model of WPC with different heights was fitted, as shown in **Fig. 9**. The equation for each group is as follows:

$$\text{C50:}\quad \varepsilon = 0.058\frac{\sigma}{E} + 62.07\left(\frac{\sigma}{E}\right)^{2.29} \tag{13}$$

$R^2 = 0.826$.

$$\text{C100:}\quad \varepsilon = 0.59\frac{\sigma}{E} + 8.6\times10^6\left(\frac{\sigma}{E}\right)^{4.62} \tag{14}$$

$R^2 = 0.993$.

$$\text{C150:}\quad \varepsilon = 0.22\frac{\sigma}{E} + 3305.72\left(\frac{\sigma}{E}\right)^{3.61} \tag{15}$$

$R^2 = 0.914$.

The relationship between parameters and height obtained through regression analysis and calculation is shown in **Fig. 10**:

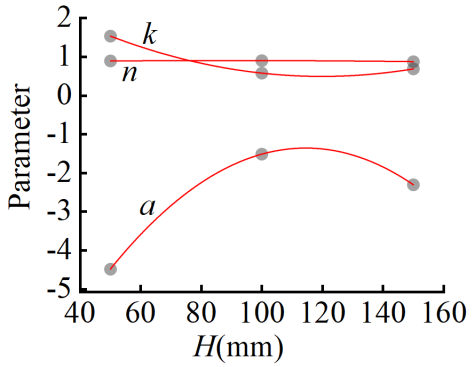

Fig. 10 Relationship between parameters and specimen height

As can be seen from the **Fig. 10**, the coefficient a initially increases and then decreases with increasing specimen height, while the coefficient k initially decreases and then increases again with the specimen height. The coefficient n basically remains unchanged. After regression calculation and analysis, the relationship between the three parameters and the height of the specimen is as follows:

$$a = -7.52\times10^{3}H^{2} + 0.17\times10^{7}H - 11.21\times10^{7} \tag{16}$$

$$n = 2.13\times10^{3}H^{2} - 0.05\times10^{7}H + 3.56\times10^{7} \tag{17}$$

$$k = -7.75\times10^{-6}H^{2} + 0.0013H + 0.85 \tag{18}$$

5.2 Analysis of size effect

The Weibull distribution (based on the theory that the weakest link in the chain will cause failure) was used to analyze the effect of specimen size on the compressive strength of WPC, and the non-parametric statistical method was adopted to calculate the size effect coefficient of WPC [24]. Weibull proposed the weakest chain theory [15], according to which the material consists of several small units and the failure of any unit in the material is considered as failure. The failure probability of the structure at any volume can be determined as follows:

$$F(\sigma) = 1 - \exp\left[\left(-\frac{V}{V_r}\right)\left(\frac{\sigma}{\alpha}\right)^{\beta}\right] \tag{19}$$

Where: V_r is unit volume, σ is uniformly distributed stress; α is the size parameter and β is the shape parameter. If both specimens conform to the Weibull distribution, the failure probability of both specimens are the same:

$$1 - \exp\left[\left(-\frac{V_1}{V_r}\right)\left(\frac{\sigma_1}{\alpha}\right)^{\beta}\right] = 1 - \exp\left[\left(-\frac{V_2}{V_r}\right)\left(\frac{\sigma_2}{\alpha}\right)^{\beta}\right] \tag{20}$$

$$\left(-\frac{V_1}{V_r}\right)\left(\frac{\sigma_1}{\alpha}\right)^{\beta} = \left(-\frac{V_2}{V_r}\right)\left(\frac{\sigma_2}{\alpha}\right)^{\beta} \tag{21}$$

$$\therefore \quad \frac{\sigma_1}{\sigma_2} = \left(\frac{V_1}{V_2}\right)^{\frac{1}{\beta}} = \left(\frac{V_1}{V_2}\right)^{S_v} = \left(\frac{H_1}{H_2}\right)^{S_h}\left(\frac{W_1}{W_2}\right)^{S_w}\left(\frac{T_1}{T_2}\right)^{S_t} \tag{22}$$

Where: S_v is the size effect coefficient, S_h is the height size effect coefficient, S_w is the width size effect coefficient; S_t is thickness size effect coefficient. Taking the logarithm of formula (18) twice, the Equation is as follows:

$$\ln\left\{-\ln\left[1 - F(\sigma)\right]\right\} = \ln V - \ln V_r + \beta\ln\sigma - \beta\ln\alpha \tag{23}$$

Since the failure probability $F(\sigma)$ and unit volume V_r are constant, $ln\,\sigma$ has a linear relationship with $ln\,V$. As $\ln T$ and $\ln W$ are constant, so $\ln H$ and $\ln\sigma$ are linear. When the width and thickness of the specimen are the same, the Equation can be written as:

$$\ln V = \ln\left(HWT\right) = \ln H + \ln W + \ln T \tag{24}$$

Therefore, the size effect coefficient can be calculated by fitting the logarithm of the compressive strength and the volume of the WPC specimen, and the height size effect coefficient can be calculated by fitting the logarithm of the compressive strength and the height of the WPC specimen with different heights. The compressive strength corresponding to percentile was estimated using a nonparametric statistical method. By counting the percentile as P_X, a set of observations can be divided into two parts, where theoretically there are X% of the observed ratio less than and (100-X) % of the observed ratio is greater than P_X. The data samples of the population are sorted in order from smallest to largest, with n being the total number of samples. Calculate i to obtain Equation (25):

$$\frac{X}{100} \geq \frac{i}{n+1} \tag{25}$$

j is defined as the smallest positive integer greater than or equal to i, and the percentile P_X is calculated by the linear interpolation method.

$$P_X = X_{j-1} + \left(X_j - X_{j-1}\right)\left[(n+1)\frac{X}{100} - (j-1)\right] \tag{26}$$

The compressive stress values corresponding to the 24 percentiles (4%, 8%, ⋯; 92%, 96%) were estimated with 3 stress values for each percentile. Linear regression analysis was conducted with the logarithm of compressive stress percentile value as ordinate and logarithm of specimen volume and height as ordinate. The slope of the line was the size effect coefficient of the percentile point.

Fig. 11(a) shows the relationship between the 24 percentiles and the volume coefficient. It can be seen from the **Fig. 11** that the volume size effect coefficient decreases with the increase of the percentiles. **Table 4** shows that the regression equation of the volume-size effect coefficient is $P < 0.05$, indicating that the regression equation is significant. The equation of the slope and intercept of t test, $|t| > t_{0.05}$, it shows that the slope is significantly different from zero, the size effect coefficient S_v is not constant. Therefore, the volume size effect coefficient S_v has a linear relationship with the percentile P_c:

$$S_v = -0.001P_c + 0.168 \tag{27}$$

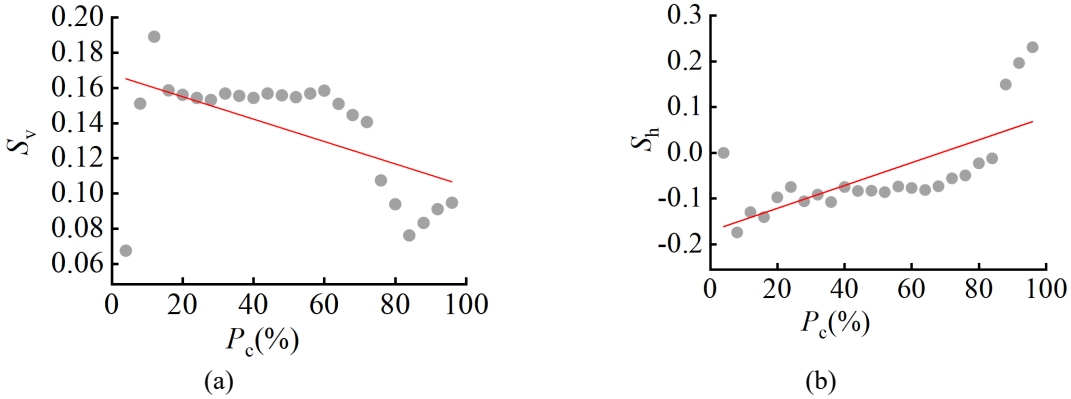

Fig. 11 Analysis of the height size effect coefficient and percentile

Fig. 11(b) shows the relationship between the 24 percentiles and the height size effect coefficient. It can be seen in **Fig. 11(b)** that the height size effect coefficient increases with the percentiles. **Table 4** shows that the regression equation of the height size effect coefficient is $P < 0.05$, indicating that the regression equation is significant. The equation of the slope and intercept of t test, $|t| > t_{0.05}$, it shows that the slope is significantly different from zero, S_h is not constant. Therefore, the height size effect coefficient S_h has a linear relationship with percentile P_c:

$$S_h = 0.002P_c - 0.171 \tag{28}$$

Table 4 Regression analysis of height size effect coefficient and percentile

	Model	Coefficient	Standard error	t	p
S_v	Intercept	0.168	0.012	13.871	0
	Slope	-0.001	0	-3.007	0.006
S_h	Intercept	-0.171	0.031	-5.573	0
	Slope	0.002	0.001	4.64	0

Table 5. shows the size effect model of different materials. It can be seen from the table that the size effect of concrete is calculated according to the ratio between the size of the specimen and the standard size, the proportion coefficient of concrete is related to the property parameters of raw materials. While studies on wood-plastic or other bamboo and wood materials are mostly based on the ratio rule of different sizes, the determination of proportion coefficient needs further research.

Table 5 Comparison of size effect of different materials

References	Materials	Size effect expression	Note
This paper	WPC	$\frac{\sigma_1}{\sigma_2}=\left(\frac{V_1}{V_2}\right)^{S_v}$, $S_v=-0.001P_c+0.168$ $\frac{\sigma_1}{\sigma_2}=\left(\frac{H_1}{H_2}\right)^{S_h}$, $S_h=0.002P_c-0.171$	
[22]	Orthogonal glulam of Larch (along grain)	$\frac{\sigma_1}{\sigma_2}=\left(\frac{L_1}{L_2}\right)^{S_L}\left(\frac{W_1}{W_2}\right)^{S_W}\left(\frac{T_1}{T_2}\right)^{S_T}$ $S_L=-0.349P_{cS}+0.278$ $S_W=0.349, S_T=0$	σ_1 and σ_2 are the compressive strength of two specimens, L_1 and L_2 are the length of those, W_1 and W_2 are the width, T_1 and T_2 are the thickness, S_L S_W and S_T are the corresponding three coefficients, P_{CS} is the percentage.
[23]	Concrete	$\frac{f_{co}}{f_c'}=\left(\frac{D}{150}\right)^{-0.112}$	f_{co} is the peak axial stress, f_c' is the compression strength of a standard concrete specimen with diameter of 150 mm, D is diameter of cylinder concrete specimen.
[24]	Concrete-filled steel tube	$\frac{\sigma_u}{\sigma_{u,150}}=\left(\frac{D}{150}\right)^{K(\xi)}$ $\xi=\alpha\frac{f_y}{f_c'}$ $K(\xi)=\begin{cases}0.092\xi^{0.46}-0.12(\xi\le 1.5)\\0(\xi>1.5)\end{cases}$	σ_u is peak stress of concrete-filled steel tube column with diameter of D, $\sigma_{u,150}$ is peak stress of concrete-filled steel tube column with diameter of 150 mm α is ratio of the steel area over the concrete area, f_y is yield strength, f_c' is peak stress of unconfined concrete column with diameter of 150 mm.
[25]	High-performance fiber-reinforced concretes (HPFRC)	$\frac{\sigma_1}{\sigma_2}=\left(\frac{V_1}{V_2}\right)^{\frac{1}{m}}$	HPFRC1 having no fiber, m=8.69, HPFRC2 containing 1.0% macro hooked fibers blended with 0.5% micro smooth fibers by volume, m=8.74.

6 Conclusions

In this paper, three groups of specimens with equal volume increase and three groups of specimens (including the previous 15) with the same cross section and equal height increase were tested for the compressive properties of WPC, and the conclusions were as follows:

(1) The compression failure modes of WPC can be mainly divided into two types: V - or Y-shaped splitting failure and detachment failure.

(2) Based on the Ramberg-Osgood model and test data, three groups of stress-strain models for WPC were obtained, and the simulated results were in good agreement with the test results.

(3) The mechanical properties of each specimen were analyzed. A negative relationship between ultimate load and volume was shown. The ultimate displacement correlated positively with height, while the ultimate load correlated negatively with height.

(4) According to Weibull brittle fracture theory, the relationship between size effect coefficient and percentile is analyzed by parametric method. The relationship between the volume size effect coefficient and percentile and the relationship between the height size effect coefficient and percentile are obtained.

(5) The development and application of WPC in the construction field and other stressed components need further research, such as the fire resistance, the influence of slenderness ratio on mechanical properties and methods of strengthening WPC components.

Acknowledgment

The writers gratefully acknowledge Yukun Tian, Chen Chen, Ben Chen, Shaoyun Zhu, Liqing Liu, Dunben Sun, Jing Cao, Yanjun Liu, Junhong Xu and others from the Nanjing Forestry University for helping.

The authors declare that we do not have any commercial or associative interest that represents a conflict of interest in connection with the work submitted.

The datasets generated and analysed during the current study are available from the corresponding author on reasonable request.

Funding Statement

This work was supported by the National Natural Science Foundation of China (No. 51878354 & 51308301); the Natural Science Foundation of Jiangsu Province (No. BK20181402 & BK20130978); 333 talent high-level project of Jiang-su Province; the Ministry of Housing and Urban-Rural science project of Jiangsu Province (No. 2021ZD10) and Qinglan Project of Jiangsu Higher Education Institutions. Any research results expressed in this paper are those of the writer(s) and do not necessarily reflect the views of the foundations.

CRediT authorship contribution statement

Yijia Guo: Investigation, Formal analysis, Writing – original draft. **Bingyu Jian**: Investigation, Formal analysis, Writing – original draft. **Haitao Li**: Conceptualization, Funding acquisition, Supervision, Investigation, Formal analysis, Writing – original draft. **Sarah Mohrmann:** Investigation, Formal analysis, Writing – original draft. **Yuanjie Li**: Supervision, Writing – review & editing.**Jiachen Lei:** Formal analysis, Writing – original draft. **Mahmud Ashraf**: Supervision, Writing – review & editing. **Jun Zhou**: Supervision, Writing – review & editing. **Xiaoyan Zheng:** Investigation, Writing – review & editing.

Conflicts of Interest

The authors affirm that, in the context of this research endeavor, there are no financial, professional, or personal interests that could potentially give rise to any conflicts of interest.

Data Availability Statement

The datasets generated and analysed during the current study are available from the corresponding author on reasonable request.

References

[1]. Dauletbek A.; Li H.; Xiong Z.; Lorenzo R. A review of mechanical behavior of structural laminated bamboo lumber. Sustainable Structures, 2021; 1(1): 000004. https://doi.org/10.54113/j.sust.2021.000004.

[2]. Jian W.; Pan H.; Xu C. Comparison and analysis of mechanical properties of wood plastic composites with different formulations. Plastics Industry, 2012; 40(02): 68-70. https://kns.cnki.net/kcms/detail/detail.aspx?FileName=SLGY201202021&DbName=CJFQ2012.

[3]. Seyyed K.H.; Shamspour M.; SafdariV.; Pourmousa S.; Ayrilmis N. The influence of popler inner and outer bark content on mechanical properties of wood/polypropylene composites. Journal of the Chilean Chemical Society, 2017; 62(1): 3365-3369. https://doi.org/10.4067/S0717-97072017000100012.

[4]. Ratanawilai T.; Taneerat K. Alternative polymeric matrices for wood-plastic composites: Effects on mechanical properties and resistance to natural weathering. Construction and building materials, 2018; 172: 349-357. https://doi.org/10.1016/j.conbuildmat.2018.03.266.

[5]. Hietala M.; Samuelsson E.; NiinimKi J.; Oksman K. The effect of pre-softened wood chips on wood fibre aspect ratio and mechanical properties of wood–polymer composites. Composites Part A: Applied Science

& Manufacturing, 2011; 42(12): 2110-2116. https://doi.org/10.1016/j.compositesa.2011.09.021.
[6]. Mathew A. P.; Oksman K.; Karim Z.; Liu P.; Naseri N. Process scale up and characterization of wood cellulose nanocrystals hydrolysed using bioethanol pilot plant. Industrial Crops and Products, 2014; 58(1): 212–219. https://doi.org/10.1016/j.indcrop.2014.04.035.
[7]. Salehpour S.; Rafieian F.; Jonoobi M.; Oksman K. Effects of molding temperature, pressure and time on polyvinyl alcohol nanocomposites properties produced by freeze drying technique. Industrial crops and products, 2018; 121: 1-9. https://doi.org/10.1016/j.indcrop.2018.04.079.
[8]. Bengtsson M.; Oksman K. Silane crosslinked wood plastic composites: processing and properties. Composites Science & Technology, 2006; 66(13): 2177-2186. https://doi.org/10.1016/j.compscitech.2005.12.009.
[9]. Koay S. C.; Subramanian V.; Chan M. Y.; Pang M. M.; Tsai K. Y.; Cheah K. H. Preparation and Characterization of Wood Plastic Composite Made Up of Durian Husk Fiber and Recycled Polystyrene Foam. Matec Web of Conferences. 2018; 152: 02019. https://doi.org/ 10.1051/matecconf/201815202019.
[10]. Turku I.; Karki T. Reinforcing wood-plastic composites with macro- and micro-sized cellulosic fillers: Comparative analysis. Journal of Reinforced Plastics and Composites. 2013; 32(22): 1746-1756. https://doi.org/10.1177/0731684413496574.
[11]. Wang H.; Wang Q.; Xie Y.; Song Y. Effects of Geometrical Shapes of Wood Particles on the Mechanical and Water-Uptake Properties of the Resulting Wood/High Density Polyethylene Composites. Advanced Materials Research. 2010; 113-116. 674-678. https://doi.org/10.4028/www.scientific.net/AMR.113-116.674.
[12]. Zhang L.; Sun J.; Yu Q.; Li R.; Zhang Y.; Wang W. Effect of hydrophobic modification of wood powder on properties of HDPE based wood plastic composite. Chemical Industry and Engineering Progress. 2020; 39(09): 3487-3493. https://doi.org/10.16085/j.issn.1000-6613.2019-1873.
[13]. Zhang X.; Gao T.; Zhang T.; Liu Q. Effect of different molecular weight polyethylene glycol on the properties of polylactic acid-based wood plastic composites. Engineering Plastics Application. 2021; 49(06): 27-30+47. https://doi.org/ 10.3969/j.issn.1001-3539.2021.06.005.
[14]. Weibull, W. The phenomenon of rupture and flow in solids. Ing. Vetenskaps Acad. Handl. 1939.
[15]. Freudenthal A.M.; Gumbel E.J. Physical and Statistical Aspects of Fatigue. Advances in Applied Mechanics 1956; 4: 117-158.
[16]. B, Z.X. Inaugural Article: Scaling theory for quasibrittle structural failure. Proc Natl Acad Sci U S A, 2004; 101(37): 13400-13407. 10.1073/pnas.0404096101
[17]. Ant Z.B.; Yavari A. Is the cause of size effect on structural strength fractal or energetic-statistical. Engineering Fracture Mechanics. 2007; 74(17): 2897-2910.
[18]. Bazant, Z.P.; Xiang Y. Size Effect in Compression Fracture: Splitting Crack Band Propagation. Journal of Engineering Mechanics. 1997; 123(2): 162-172.
[19]. Carpinteri, A.; Ferro G.A.; Chiaia B. Multifractal scaling law for the nominal strength variation of concrete structures. Applied Mechanics & Materials. 1993; 725-726: 214-219.
[20]. Carpinteri A.; Chiaia B. Multifractal scaling laws in the breaking behaviour of disordered materials. Chaos Solitons & Fractals. 1997; 8(2): 135-150.
[21]. Ramberg W.; Osgood W. R. Description of stress-strain curves by three parameters (No. NACA-TN-902). 1943.
[22]. Gong Y.; Ye Q.; Wu G.; Ren H.; Guan C. Effect of size on compressive strength along grain of domestic orthogonal glulam larch. Wood Science and Technology. 2021; 35(01): 42-46. https://doi.org/10.12326/j.2096-9694.2020019.
[23]. Chen P.; Liu C.; Wang Y. Size effect on peak axial strain and stress-strain behavior of concrete subjected to axial compression. Construction and Building Materials, 2018; 188: 645-655. https://doi.org/10.1016/j.conbuildmat.2018.08.072.
[24]. Chen, P.; Wang Y.;Zhang, S. Size effect prediction on axial compression strength of circular cfst columns. Journal of Constructional Steel Research, 2020; 172: 106221. https://doi.org/10.1016/j.jcsr.2020.106221.
[25]. Nguyen D. L.; Thai D. K.; Ngo T. T.; Tran T. K.; Nguyen, T. T. Weibull modulus from size effect of high-performance fiber-reinforced concrete under compression and flexure. Construction and Building Materials, 2019; 226(30): 743-758. https://doi.org/10.1016/j.conbuildmat.2019.07.234.